

Application of naphthalene diimide in biotechnology

著者	Takenaka Shigeori
journal or publication title	Polymer Journal
volume	53
number	3
page range	415-427
year	2020-11-10
URL	http://hdl.handle.net/10228/00008242

doi: <https://doi.org/10.1038/s41428-020-00434-2>

Application of naphthalene diimide in biotechnology

Shigeori Takenaka

Department of Applied Chemistry, Kyushu Institute of Technology, Kitakyushu 804-8550 Japan

Abstract

Naphthalene diimide (NDI) is an electron-deficient, robust, and planar molecule. These characteristics make it highly applicable for electronic devices that employ its electric character, for imide group-based supramolecular materials that utilize its hydrogen-bonding, or for sensing materials with a combination of functional groups. Water-soluble NDI binds to the DNA duplex via threading intercalation mode. This has provided unique DNA analytical techniques, functional DNA polymers, and supramolecular polymers. The ferrocene-containing NDI, having electrochemically active sites, has been applied to an electrochemical gene detection system and also utilized in the precision analysis of genes and single nucleotide polymorphisms. Recently, a DNA quadruplex was identified as one of the non-canonical DNA structures formed by guanine-quartet (G4). The latter serves as one of the control units of gene expression and is connected with cancer development. A stable complex was formed between electron-deficient NDI and the electron-rich G4 planes. Since G4 stabilizer is recognized as an anticancer agent with fewer side-effects, NDI derivatives may serve as potential candidates for anticancer therapeutics or for designing a unique cancer-detection system.

Introduction

Naphthalene diimide (NDI, Fig. 1a) is a thermally stable, robust, and electron deficient aromatic planar molecule that shows reversible reduction and oxidation (redox) reaction. NDI utilizes a flexible display for n-type semiconducting material, field effect transistor (FET), or solar energy converter

using its photo-induced electron transfer character [1-3]. Supramolecular formation and its application using imide moieties utilize hydrogen bonding, π -stacking ability of the aromatic plane, the van der Waals interaction, or their combinations [1-3]. Water-soluble NDI is known to bind to DNA duplex with the help of threading intercalation, wherein NDI inserts between adjacent base pairs [4]. Core part of the DNA duplex forms hydrophobic base pairs and unwinding of this duplex creates space to accept the aromatic moiety. During intercalation, one of the substituents connected with the amide parts of NDI passes through the adjacent base pairs and the two NDI substituents project forward from the major and minor grooves. The term “threading intercalation” is derived from such a binding process [5]. These substituents act as anchors and stabilize the NDI-DNA duplex complex. DNA analysis was performed to achieve the supramolecular DNA polymers owing to their unique binding manner [2]. Recently, DNA quadruplexes have been identified as a non-canonical DNA structure formed by guanine (G)-quartet and is one of the control units associated with cancer progression. The G-quartet structure is found on the telomere DNA at the termini of chromosome or on the regulatory parts of tumor-associated genes, thus gaining popularity among the anticancer therapeutics [6]. G-quartet structure in the DNA is formed by consecutive folding of four Gs via hydrogen bonding [7]. Guanine has the lowest oxidation potential and is easy to oxidize; it accepts one electron of NDI and thus, charge transfer is expected between NDI and G-quartet planes to form a stable complex in this interaction [8]. This review briefly focuses on the research conducted on the interaction between NDI and DNA quartets so far. **Table 1 and 2 shows the functionalized NDI derivatives developed by Takenaka’s group with some physical data.**

Characteristics of NDI

NDI is a robust electron-deficient planar molecule with a reversible redox activity. It has D_{2h} in point group and shows the electron transitions among dipoles for the long and short axes [9]. Electron

transition at 300-400 nm (band I) at the long axis and the electron transition at 200-250 nm (band II) at the short axis is due to $\pi \rightarrow \pi^*$ transition of $S_0 \rightarrow S_1$. Figure 1b shows the typical spectra pattern of NDI with absorption and emission maxima at 383 nm and 390 nm, respectively. It is known that Stokes shift of this spectrum is 7 nm and its fluorescence lifetime is 20 ps [10]. One electron reductant shows emission at 473 nm [9]. NDI of R-alkyl moieties shows intermolecular stacking and aggregate formation under the crystal or apolar solvent states, where broad absorption is observed over 400 nm (Fig. 1 c) [11]. Figure 1d shows the expected cyclic and differential pulse voltammogram of NDI. NDI accepts two electrons at redox potentials of ca. -0.76 V and -1.00 V [12]. This reduction is reversible and this property is exploited for free-electron carrying to permit functioning in the n-type semiconducting material [1, 2].

Interaction of NDI with DNA duplex

NDI, carrying the dimethylaminoethyl moieties at its imido parts, dissolves neutral buffer where it behaves as a divalent cation [4]. It disperses in its monomer form at micromolar level. The NDI shows absorption maximum at 383 nm (Fig. 2a and Fig. 1a); and a large hypochromic effect and small red shift are observed upon the addition of sonicated calf thymus DNA with isosbestic point (Fig. 2a). Red shift is derived from an exciton interaction, e.g. two chromophores between NDI and nucleic base pairs show stacking interaction and two energy levels are formed by Davydov splitting. The lower energy level becomes an allowed transition and thus, the absorption peak shifts towards longer wavelength. Additionally, NDI and nucleic base pairs are stacked with each other, they are nullified, and the sum of transition moments becomes diminished. Since its square is correlated with the oscillator strength (absorption intensity), a hypochromic effect is observed in this system. Threading intercalation model of NDI for DNA duplex has been shown in Fig. 2c and 2d; and its model is in agreement with this spectral behavior. Threading intercalation of NDI was demonstrated with cyclic

bis-NDI by Iverson's group [13]. Binding behavior of the NDI derivative with the DNA duplex was analyzed by spectral change of NDI upon addition of the DNA duplex. Isosbestic point showed the existence of only two states between the unbound and bound forms (Fig. 2a). Absorption change at specific wavelength upon addition of DNA gives a binding ratio under varied DNA concentrations (binding affinity, K , and binding site size, n , which means how many base pairs are bound to a single molecule of NDI) and is obtained with this spectra change by Scatchard analysis using McGhee & von Hippel theory as shown in the following equation [14].

$$\frac{\nu}{c} = K(1 - n\nu) \left(\frac{1 - n\nu}{1 - (n-1)\nu} \right)^{n-1}$$

Here n is the maximum number of NDIs bound dsDNA per base pair, c is the free NDI concentration, K is the observed binding constant, and ν represents the moles of NDI bound per base pair. McGhee and von Hippel also developed the equation under cooperative interaction included cooperative parameter, ω [14]. Concentration of sonicated calf thymus polymeric DNA has been estimated per base pairs. Ordinary NDI derivatives have around 10^5 M^{-1} order of binding constant and n is two, which is in agreement with the excluded-site model [5]. The binding constant was also detected using isothermal titration calorimetric (ITC) technique because of the heat change observation after interaction between NDI and DNA [15].

Kinetics of the threading intercalation of the NDI-DNA duplex are measured as the absorption change of stopped flow instruments, implying a slow process compared with the classical intercalating agent ethidium bromide. It is known that association and dissociation rate constants are $k_a=10^5 \text{ M}^{-1}\text{s}^{-1}$ and $k_d=0.1 \text{ s}^{-1}$, respectively; and thus binding constant obtained from $K=k_a/k_d=10^6 \text{ M}^{-1}$, is in agreement with the value from Scatchard analysis [5]. The NDI binding to the AT polymer DNA poly[d(A-T)]₂ is relatively slower than that seen in the GC polymer DNA poly[d(G-C)]₂. In contrast, NDI dissociation from poly[d(G-C)]₂ is slower than that from poly[d(A-T)]₂ and gives a similar binding affinity between AT and GC polymers, resulting in no nucleic base selectivity [5].

DNA duplex is a chiral polymer known to generate negative and positive Cotton effect at 240 nm and 260 nm, respectively, as recorded in the circular dichroism (CD) spectra. NDI shows negative CD signal around 383 nm even in achiral molecules after being bound to the DNA duplex with threading intercalation (induced CD, Fig. 2b). This comes from the stereochemical fixing under chiral environment of DNA duplex [4].

The threading intercalation of NDI for DNA duplex also causes unwinding of the DNA helix. This behavior is demonstrated by an unwinding experiment using supercoiled plasmid DNA and the unwinding angle is 14° with an ordinary intercalator such as acridine [16].

Ferrocenyl naphthalene diimide (FND) derivatives

A series of naphthalene diimide derivatives carrying ferrocene moieties at the substitution termini from amido parts (FNDs) was synthesized by Takenaka's group (Fig. 3a) [17]. These derivatives are bound to DNA duplex with 10^5 - 10^6 M⁻¹ order. While the FNDs have no nucleic base selectivity, they have a higher preference for DNA duplex over single stranded DNA. Takenaka's group has developed an electrochemical gene detection technique that exploits FND coupled with DNA probe-immobilized electrode [17]. This concept is shown in Fig. 3b: (i) DNA probe (DNA fragment carrying a sequence complementary to the DNA of interest) is immobilized on the electrode. (ii) In the next step of hybridization, the electrode is dipped into a solution containing a mixture of DNA fragments extracted from the sample and is heated and subsequently cooled slowly. When target DNA is present in this sample, DNA duplex is formed with the DNA probe on the electrode. This electrode generates potential in the electrode containing FND and the redox current is observed. Redox peak based on ferrocene is observed in cyclic or differential pulse voltammogram. Since the intensity of the peak current depends on the amount of DNA duplex, the amount of target DNA in the sample is indirectly used to estimate this intensity. FND bound to DNA duplex per two base pairs and the increased DNA

duplex directs the current resulting in **subpico molar concentration detection**. Takenaka's group measured the current before hybridization and estimated the DNA amount immobilized on the electrode. Since FND behaves as a divalent cation in an acidic electrolyte and DNA is a polyanion, the current obtained here is expected to correlate with the amount of DNA immobilized at the electrode and these values could be used as a nominalization of the individual DNA-immobilized electrode. Thus, one can estimate the amount of hybridized DNA per amount of DNA probe immobilized at an individual electrode. Takenaka's group has reported electrochemical gene detection as an application of the FND-based electrochemical hybridization assay [18-25].

In particular, since FND intercalates adjacent base pairs of the DNA duplex, it does not bind to the mismatched base pair site and its neighborhood owing to steric straining [18]. This employs mismatched bases such as single nucleotide polymorphism (SNP) detection using this system. This system not only permits simple mismatched DNA detection, but also allows discrimination between the heterozygous and homozygous conditions [19-21, 23]. SNPs of lipoprotein lipase (LPL) gene were successfully detected with discrimination of heterozygous and homozygous states using this system [19, 20]. This system is also employed to multi electrode as an electrochemical DNA chip [26]. Takenaka's group synthesized FND derivatives carrying variable linker length and/or connecting part of ferrocene (Fig. 3a) [27]. The redox potential of FND varies depending upon the electron donating or withdrawing characters of connecting part to ferrocene; strong electron donating character of FND shows the potential peak at a more negative potential. Furthermore, NDI derivative carrying four ferrocene moieties, NDI8 (Fig. 3a), was also synthesized and implied to electrochemical gene detection [28].

Supramolecular gene detection combined with NDI, ferrocene, and/or β -cyclodextrin

It is known that β -cyclodextrin (β -CD) is a hydrophobic molecule carrying lipophilic pockets and

includes lipophilic molecules with a relevant size, such as ferrocene or adamantane. The complex formation constant of β -CD with ferrocene is 10^3 M^{-1} . FND binds to the DNA duplex with threading intercalation and thus, the ferrocene parts of FND are located on the major and minor grooves of the duplex. When β -CD caps these ferrocenes on the DNA grooves, further stabilization of the FND-DNA duplex complex is expected. This behavior was achieved by FND7 carrying a shorter linker chain (Table 1 and Fig. 4a) [29]. Since the ferrocene of FND is hard to oxidize when included with β -CD, diminished and positively shifted peak current was observed. Improved detection limit was achieved by this complex stabilization despite of the disadvantage in the electrochemical detection system. On the other hand, it is known that the β -CD includes adamantane with a higher complex formation constant of 10^4 M^{-1} in comparison to ferrocene. Therefore, ferrocenyl β -CD (Fc- β -CD) includes adamantane and its ferrocene part protrudes after coupling with adamantane. Based on this behavior, NDI derivatives carrying adamantane i.e., NDI-Ad moieties were synthesized. A novel electrochemical DNA detection system was constructed with NDI-Ad and Fc- β -CD. Target DNA was allowed to hybridize with DNA probe and NDI-Ad bound to DNA hybrid region and the subsequently capped adamantane moieties with Fc- β -CD. In this process, ferrocene part of Fc- β -CD protruded after including to NDI-Ad bound to DNA duplex region, resulting in the generation of an electrochemical signal of ferrocene part (Table 1 and Fig. 4c). When this process was performed at the electrode, new electrochemical gene detection strategy was achieved [30].

Interestingly, FND2 carrying the linker chains was included with β -CD. However β -CD was protruded upon FND2 binding with the DNA duplex. This behavior provided increased current with negative-side shift and allowed electrochemical discrimination between the duplex and single stranded DNA under homogenous media conditions. Homogenous electrochemical detection of DNA duplex was achieved by voltage shift as an index (Table 1 and Fig. 4b). Finally, electrochemical real-time PCR was carried out using this system as an example of the periodontal disease bacteria

Porphyromonas gingivalis and the detection limit of this system was 2.7 nM with signal linearity from lower PCR cycle number than that in the case of the ordinary PCR using SYBR Green [31]. Electrochemical gene detection is achieved by the system where intramolecular inclusion of β -CD-ferrocene complex collapses after DNA duplex binding. NDI carrying ferrocene and β -CD, FNC1 was synthesized to implement this idea [32]. The intramolecular inclusion complex of ferrocene with the β -CD part was observed; and the redox current of FNC1 decreased with positive shift compared to ferrocene alone (Table 1 and Fig. 4d). FNC1 showed a reduced binding affinity of 10^5 M^{-1} with $n=2$ driven from DNA binding after collapse of the intramolecular complex. Thus, signal-on electrochemical detection of PCR products, which have the potential for greatly improved sensitivity because of zero background signal, was achieved under a homogeneous electrolyte.

NDI carrying dicobalt hexacarbonyl complex at the substituent termini

NDI binds to DNA duplex with threading intercalation mode and forms a stable complex. FND binds to DNA duplex every two base pairs and can be regarded as a one-dimensional ferrocene-array tracing the DNA duplex. On these grounds, NDI provides a tool to sequentially arrange a variety of functional molecules on the one-dimensional DNA duplex. Dicobalt hexacarbonyl complex is known to be stable in water and be an infrared (IR) active compound, showing typical absorption at $2100\text{-}2020 \text{ cm}^{-1}$, which does not overlap with IR absorption for any living organism. Thus, DNA duplex can detect IR absorption intensity using this derivative. Takenaka's group synthesized NDI carrying dicobalt hexacarbonyl complex at the substituent termini (Table 2) [33]. This NDI had a binding constant order of 10^6 M^{-1} with a site size of 2. Fourier Transform Infrared Reflection-Absorption Spectroscopy (FT-IR RAS) of DNA probe-immobilized gold surface was measured before and after hybridization with sample DNA. IR absorption intensity at $2100\text{-}2020 \text{ cm}^{-1}$ was

elevated with an increase in the amount of target DNA [3]. Since this IR absorption is silent in living cells, this system can be implied to the IR imaging of DNA duplex *in vivo*.

DNA nanowire and DNA rod using NDI

In the use of NDI carrying glucose as the reducing sugar (NDI-DS), glucose is arranged on DNA duplex surface unidimensionally. NDI-DS has a binding constant of 10^6 M^{-1} ($n=2$) and since DNA duplex bound to NDI-DS is treated by Tollens' reagent, silver nanowires should form a DNA duplex template (Table 2 and Fig. 5a) and convert to gold nanowires [34]. DNA works as a bridge between the two electrodes using a microfluidic system and nanowires can be formed using Tollens' reagent. Since NDI-DS does not form a stable complex with single stranded DNA, only DNA duplex is expected to convert to the nanowire. Yasuda et al. achieved the detection system of nuclease using microelectrode bridged single stranded DNA having DNA duplex region and subsequently its nanowire formation [35]. FNC2 bound to the DNA duplex with a binding constant of 10^5 M^{-1} , binding site size of 4, and positive cooperative binding (Cooperativity parameter is 14). AFM measurement of linear plasmid DNA recorded a rod shape DNA or nanorod after treatment with FNC2 (Table 1 and Fig. 5b). This might have been driven by the intermolecular inclusion of ferrocene with β -CD of FNC2 bound to the DNA duplex every four base pairs [36].

Immobilization of DNA duplex by NDI as a molecular staple

Thiol or disulfide adsorbs to the bare gold surface to form a strong bond in the process of chemisorption. DNA immobilization on the gold electrode is carried out between the thiolated oligonucleotide and the pretreated gold surface. This behavior has been analyzed in detail by Steel and Tarov [37]. NDI carrying dithiolane or thiol moieties at the substituent termini (Table 2) binds to the DNA duplex with threading intercalation mode, where it is projected outwards from its major and

minor grooves. When gold surface was treated with this complex, both dithiolane or thiol moieties were bound to the gold surface and DNA duplex also immobilized topologically, where DNA duplex was not immobilized directly. On the other hand, DNA duplex was fixed on the surface like being stapled to the gold surface as shown in Fig. 5c. NDI should prove the general method to immobilize bare DNA duplex on the sold surface. DNA probe connected with DNA duplex region was immobilized on the gold electrode and target DNA detected by DNA probe part using an FND-based hybridization assay [38, 39]. Using a longer DNA duplex region to be immobilized on the gold electrodes gives a greater number of immobilization sites (large number of NDI-SH is concentrated in the DNA duplex region), and helps to achieve robust DNA immobilization.

DNA quadruplex detection by NDI derivatives

DNA fragments containing guanine (G) contiguous sequence forms quadruplex through G-quartet (Fig. 6a) plane formed from hydrogen bonding of four guanine bases. This has been observed at the telomere repeating sequence of the chromosomal termini (TTAGGG repeating sequence in the case of humans) [40]. Different structures of quadruplex DNA are shown in Fig. 6b; the hybrid type quartet exists in the human telomere DNA tetraplex [40]. Recently, such a structure was observed at the promoter region of cancer gene. The stabilization of such structures is anticipated to be effective as a novel cancer treatment strategy [41]. Since NDI is electron deficient aromatic molecule and G-quartet provides electron rich aromatic plane, stable stacking interaction is observed between these molecules. Thus, NDI is expected to be the effective ligand for DNA tetraplex and many reports support this theory [42]. The expected stacking interaction manner is demonstrated by the X-ray crystal structure of the DNA tetraplex and NDI derivative carrying the four substituents (Fig. 6d) [43]. FND binds to the DNA tetraplex with high affinity facilitating electrochemical detection of DNA tetraplex. Electrochemical telomerase assay was conducted by the elongated telomeric DNA using FND7 (Table

1) [44, 45]. Takenaka's group tested all of FND derivatives suitable for the electrochemical telomerase assay and FND3 was revealed to be the most effective probe in this system. Since the cancer cells harbor telomerase activity, cancer diagnosis is possible using this electrochemical telomerase assay. The principle of this system is shown in Fig. 7. TS (telomerase substrate)-primer is immobilized on the electrode through Au-S chemisorption. Protein fraction extracted from the sample cell is dipped on this sensor electrode. When this fraction possesses telomerase activity, TS-primer elongates on the electrode. The electrochemical measurement of the electrode was measured in an electrolyte containing KCl and FND3, where the elongated DNA formed the DNA tetraplex. FND3 was bound to the DNA tetraplex and FND3 was concentrated on the electrode. The current increased with rise in the amount of FND3, amount of DNA tetraplex formation, or telomerase activity mass. Oral cancer diagnosis employing this technique has been accomplished as a collaborative research with Kyushu Dental University [46, 47].

Furthermore, NDI carrying two substituents binds to the DNA duplex with threading intercalation and requires discrimination between DNA duplex and DNA tetraplex. Neidle's group synthesized the NDI derivatives carrying tri- (CM03) or tetra-substituents (MM41) that showed improved preference for the DNA tetraplex (Fig. 8a, 8b) [48]. This can be ascribed to the inhibition of DNA duplex binding in the presence of steric hindrance due to additional substituent(s) and to the anchoring of substituents located at the four grooves of DNA tetraplex. Neidle's group also demonstrated that tri-substituted NDI, CM03, is effective for Pancreatic Ductal Adenocarcinoma (PDAC) [48]. Takenaka's group synthesized tetra-substituted NDI, tFND1, tFND2 (Table 1 and Fig. 3a) that improved preference for the DNA tetraplex over duplex and have been applied to the electrochemical telomerase assay [49].

Enhancing the preference for DNA tetraplex was achieved with cyclic NDI, cNDI (Table 1 and Fig. 8c) [50]. The cNDI derivative was synthesized by linkage between the two substituents from amide parts of NDI as shown in Table 2 and it inhibits the threading intercalation for DNA duplex with

linkage chain, whereas cNDI binds to DNA tetraplex through the stacking G4-tetraplex interaction. On the other hand, cNDI leads to the expression of DNA tetraplex preference with binding to DNA tetraplex with similar binding affinity for noncyclic NDI, but cNDI was only diminishing the binding affinity for DNA duplex. This strategy has been extended to perylene diimide (PDI) and shows a higher preference for the DNA quadruplex [51]. To estimate the binding parameters for DNA tetraplex and duplex to cNDI, spectroscopic titration and Scatchard analysis were carried out. cNDI has an absorption maximum at 383 nm and large hypochromic and small red shifts were observed upon the addition of the DNA tetraplex. The binding constant and binding number values were estimated to be 10^6 M^{-1} and 2, respectively, and were in agreement with those for DNA duplex. This indicates that the effect of the NDI linker chain is not dominant for DNA tetraplex binding. In contrast, the absorption spectra of cNDI displayed only a small decrease in absorption intensity. Here, though being hard to estimate, the binding affinity constant was roughly estimated to be in the order of 10^4 M^{-1} order by Benesi-Hildebrand analysis. To obtain binding affinity parameters for DNA tetraplex and duplex more precisely, the isothermal titration calorimetry (ITC) technique was applied in this system. Consequently, a binding affinity for the DNA tetraplex observed was similar to that achieved by Scatchard analysis. However, significant heat change was not achieved for DNA duplex. These results suggested that selectivity for DNA tetraplex was 100-times higher than for that for the DNA duplex. Binding site size in the binding of cNDI with DNA tetraplex was two, indicating that cNDI bound to DNA tetraplex from upper and lower sites. While introducing ferrocene to cNDI, electrochemical DNA tetraplex detection is to be achieved. Takenaka's group synthesized cFND1-3 (Fig. 3a) and demonstrated the improved preference for DNA tetraplex with 10^6 M^{-1} order binding and successfully achieved electrochemical detection of DNA tetraplex [52].

Recently, significance of high level gene regulation was revealed by the cluster similar to a telomere G4 repeat in the chromosomal DNA tetraplex. Specific ligand for DNA tetraplex clusters is important

to regulate or analyze such G4 cluster regions (Table 2). Takenaka's group also synthesized cNDI dimers carrying the varied linker length that are expected to stabilize such DNA quadruplex clusters (Fig. 8d) [53].

Conclusion

In this review, the water-soluble NDI derivatives were discussed in the context of their DNA binding behavior and functions. These techniques allow the electrochemical detection or IR analysis. Using the NDI derivatives, DNA nanowires or DNA nanorods were prepared as examples of functionalized DNA duplexes. Recently, it has been shown that NDI derivatives are good candidates for functionalized ligand for DNA tetraplex. Application of NDIs will open the use of DNA tetraplexes as analytical tools, or approaches that are based on telomerase activity or cancer diagnosis using drugs with a fewer side effect. Although NDI molecules have been studied in the past in context of electronic materials or light conversion materials, the future foresees their use in the field of biotechnology.

Acknowledgment

I appreciate the significant contribution made by researchers who appears in the reference papers of Takenaka's group. I thank Dr. Zou Tingting for preparing a conceptual diagram of figures according to my idea and thank Dr. Satoshi Fujii for the simulation of molecular modeling of threading intercalation complex of Fig. 2c&d. Finally, I thank Dr. Shinobu Sato for engaging discussion and support.

References

- 1) S. V. Bhosale, C. H. Jani, and S. J. Langford, *Chem. Soc. Rev.*, **37**, 331-342 (2008).
- 2) M. A. Kobaisi, S. V. Bhosale, K. Latham, A. M. Raynor, S. V. Bhosale, *Chem. Rev.*,

- 116, 11685-11796 (2016).
- 3) A. Das and S. Ghosh, *Chem. Commun.*, 52, 6860-6872 (2016).
 - 4) S.-F. Yen, E. J. Gabbay, and W. D. Wilson *Biochemistry*, 21, 2070-2076 (1982).
 - 5) F. A. Tanious, S.-F. Yen, and W. D. Wilson, *Biochemistry*, 30, 1813-1819 (1991).
 - 6) T. Ou, Y. Lu, J. Tan, Z. Huang, K.-Y. Wong, and L. Gu, *ChemMedChem.*, 3, 690-713 (2008).
 - 7) D. Yang and K. Okamoto, *Future Med. Chem.*, 2, 619-646 (2010).
 - 8) V. Pirota, M. Nadai, F. Doria, and S. Richter, *Molecules*, 24, 426 (2019).
 - 9) J. Gawronski, M. Brzostowska, K. Kacprzak, H. Kolbon, and P. Skowronek, *Chirality*, 12, 263-268 (2000).
 - 10) S. Green and A. Fox, *J. Phys. Chem.*, 99, 14752-14757 (1995).
 - 11) F. Salerno, J. A. Berrocal, A. T. Haedler, F. Zinna, E. W. Meijer, and L. D. Bari, *J. Mater. Chem. C.*, 5, 3609-3615 (2017).
 - 12) G. Andric, J. F. Boas, A. M. Bond, G. D. Fallon, K. P. Ghiggino, C. F. Hogan, J. A. Hutchison, M. A.-P. Lee, S. J. Langford, J. R. Pilbrow, G. J. Thoup, and C. P. Woodward, *Aut. J. Chem.*, 57, 1011-1019 (2004).
 - 13) Y. Chu, D. W. Hoffman, B. L. Iverson, *J. Am. Chem. Soc.*, 131, 3499-3508 (2009).
 - 14) J. D. McGhee and P. H. von Hippel, *J. Mol. Biol.*, 86, 469-489 (1974).
 - 15) R. E. McKnight, A. B. Gleason, J. A. Keyes, and S. Sahabi, *Bioorg. Med. Chem. Lett.*, 17, 1013-1017 (2007).
 - 16) W. D. Wilson, R. L. Jones, *Intercalation Chemistry*, M. S. Whittingham, A. J. Jacobson (Eds), Academic Press, New York, 1982, p. 445-510.
 - 17) S. Takenaka, K. Yamashita, M. Takagi, Y. Uto, and H. Kondo, *Anal. Chem.*, 72, 1334-1341 (2000).

- 18) K. Yamashita, M. Takagi, H. Kondo, and S. Takenaka, *Anal. Biochem.*, 306, 188-196 (2002).
- 19) H. Miyahara, K. Yamashita, M. Kanai, K. Uchida, M. Takagi, H. Kondo, and S. Takenaka, *Talanta*, 56, 829-835 (2002).
- 20) T. Nojima, K. Yamashita, A. Takagi, M. Takagi, Y. Ikeda, H. Kondo, and S. Takenaka, *Anal. Sci.*, 19, 79-83 (2003).
- 21) T. Nojima, K. Yamashita, A. Takagi, Y. Ikeda, H. Kondo, and S. Takenaka, *Anal. Sci.*, 21, 1437-1441 (2005).
- 22) S. Sato, K. Hokazono, T. Irie, T. Ueki, M. Waki, T. Nojima, H. Kondo, and S. Takenaka, *Anal. Chim. Acta*, 578, 82-87 (2006).
- 23) N. Ishikawa, T. Miya, K. Mizumoto, K. Ohuchida, E. Nagai, K. Yamaguchi, M. Amano, S. Takenaka, and M. Tanaka, *Cancer Genomics Proteomics*, 3, 47-54 (2006).
- 24) S. Sato, M. Tsueda, Y. Kanezaki, and S. Takenaka, *Anal. Chim. Acta*, 715, 42-48 (2012).
- 25) K. Harahuchi, S. Sato, M. Habu, N. Yada, M. Hayakawa, O. Takahashi, I. Yoshioka, K. Matsuo, K. Tominaga, and S. Takenaka, *Electroanalysis*, 29, 1596-1601 (2017).
- 26) S. Sato, T. Saeki, T. Tanaka, Y. Kanezaki, M. Hayakawa, K. Haraguchi, M. Kodama, T. Nishihara, K. Tominaga, S. Takenaka, *Appl. Biochem. Biotechnol.*, 174, 869-879 (2014).
- 27) S. Sato and S. Takenaka, *J. Organomet. Chem.*, 693, 1177-1185 (2008).
- 28) S. Sato, M. Tsueda, and S. Takenaka, *J. organomet. Chem.*, 695, 1858-1862 (2010).
- 29) S. Sato, T. Nojima, M. Waki, and S. Takenaka, *Molecules*, 10, 693-707 (2005).
- 30) S. Sato, T. Nojima, and S. Takenaka, *J. Organomet. Chem.*, 689, 4722-4728 (2004).
- 31) H. Takenaka, S. Sato, and S. Takenaka, *Electroanalysis*, 25, 1827-1830 (2013).
- 32) S. Watanabe, S. Sato, K. Ohsuka, and S. Takenaka, *Anal. Chem.*, 83, 7290-7296

- (2011).
- 33) K. Ohtsuka, K. Komizo, and S. Takenaka, *J. Organomet. Chem.*, **695**, 1281-1286 (2010).
- 34) K. Komizo, H. Ikeda, S. Sato, and S. Takenaka, *Bioconjugate Chem.*, **25**, 1547-1555 (2014).
- 35) T. Himuro, R. Araki, S. Sato, S. Takenaka, T. Yasuda, *IEEEJ Transactions on Sensors and Micromachines*, **36**, 425-431 (2016).
- 36) S. Sato, Y. Umeda, S. Fujii, and S. Takenaka, *Bioconjugate Chem.*, **26**, 379-382 (2015).
- 37) A. B. Steel, T. M. Heme, M. J. Tarlov, *Anal. Chem.*, **70**, 4670-4677 (1998).
- 38) S. Sato, A. Hirano, and S. Takenaka, *Anal. Chimica Acta*, **665**, 91-97 (2010).
- 39) S. Sato, K. Yamamura, and S. Takenaka, *Electroanalysis*, **25**, 1831-1839 (2013).
- 40) T. Tian, Y.-Q. Chen, S.-R. Wang, and X. Zhou, *Chem.*, **4**, 1314-1344 (2018).
- 41) J. Spiegel, S. Adhikari, and S. Balasubramanian, *Trends Chem.*, **2**, 123-136 (2020)..
- 42) M. P. O'Hagan, J. C. Morales, and M. C. Galan, *Eur. J. Org. Chem.*, 4995-5017 (2019).
- 43) G. N. Parkinson, F. Cuenca, S. Neidle, *J. Mol. Biol.*, **381**, 1145-1156 (2008).
- 44) S. Sato, H. Kondo, T. Nojima, and S. Takenaka, *Anal. Chem.*, **77**, 7304-7309 (2005).
- 45) S. Sato, and S. Takenaka, *J. Inorg. Biochem.*, **167**, 21-26 (2017).
- 46) K. Mori, S. Sato, M. Kodama, M. Habu, O. Takahashi, T. Nishihara, K. Tominaga, and S. Takenaka, *Clinical Chem.*, **59**, 289-295 (2013).
- 47) M. Hayakawa, S. Sato, I. Diala, M. Kodama, K. Tomoeda-Mori, K. Haraguchi, K. Tominaga, and S. Takenaka, *Electroanalysis*, **28**, 503-507 (2016).
- 48) C. Marchetti, K. G. Zyner, S. A. Ohnmacht, M. Robson, S. M. Haider, J. P. Morton, G. Marsico, T. Vo, S. Laughlin-Toth, A. A. Ahmed, G. D. Vita, I. Pazitna, M. Gunartnam, R. J. Besser, A. C. G. Andrade, S. Diocou, J. A. Pike, D. Tannahill, R. B. Pedley, T. R.

- J. Evans, W. D. Wilson, S. Balasubramanian, S. Neidle, *J. Med. Chem.*, **61**, 2500-2517 (2018).
- 49) S. Sato, A. Kajima, H. Hamanaka, S. Takenaka, *J. Organomet. Chem.*, **897**, 107-113 (2019).
- 50) Y. Esaki, M. M. Islam, S. Fujii, S. Sato, and S. Takenaka, *Chem. Commun.*, **50**, 5967-5969 (2014).
- 51) S. Vasimalla, S. Sato, F. Takenaka, Y. Kurose, and S. Takenaka, *Bioorg. Med. Chem.*, **25**, 6404-6411 (2017).
- 52) S. Kaneyoshi, T. Zou, S. Ozaki, R. Takeuchi, A. Udou, T. Nakahara, K. Fujimoto, S. Fujii, S. Sato, and S. Takenaka, *Chem. Eur. J.*, **26**, 139-142 (2020).
- 53) R. Takeuchi, T. Zou, D. Wakahara, Y. Nakano, S. Sato, and S. Takenaka, *Chem. Eur. J.*, **25**, 8691-8695 (2019).

Figure Legends

Figure 1. (a) Chemical structure of naphthalene diimide, NDI, and its reductant. (b) Expected electronic transition spectra of NDI under polar (solid line) and apolar (broken line) solvents and the electronic transition direction of π - π^* transition bands I and II. (c) Expected excitation (solid line) and emission spectra (broken line) of NDI with the emission spectra of its reductant. (d) Expected cyclic (upper panel) and differential pulse voltammogram (lower panel) of NDI.

Figure 2. (a) Chemical structure of NDI carrying dimethylaminoethyl moieties and its

electron transition spectra upon addition of sonicated calf thymus DNA (from upper to lower panels) and (b) circular dichroism (CD) spectra of sonicated calf thymus DNA in the absence or presence of the NDI derivative. Side view (c) and top view (d) of the molecular modeling of DNA duplex-NDI complex showing the threading mode of intercalation

Figure 3. Concept of electrochemical hybridization assay using FNDs, 1-8 sa shown in Table 1.

Figure 4. Electrochemical DNA detection based on supramolecular formation: (a) Stabilization of the FND-DNA duplex complex with β -cyclodextrin (β -CD), (b) collapse of β -CD-FND complex after threading intercalation, (c) complex formation of the DNA duplex with adamantyl NDI (NDI-Ad) and subsequently with ferrocenyl cyclodextrin (Fc- β -CD); and (d) electrochemical detection of DNA duplex with FND carrying β -CD (FNC1) under homogenous medium (collapse of intramolecular inclusion complex of FNC1 after its DNA duplex binding).

Figure 5. (a) Silver nanowire formation of the DNA duplex binding of NDI carrying glucose units (NDI-DS) and subsequently Tollens' reaction. (b) Nanorod formation of DNA duplex with FND2. (c) Immobilization of bare DNA duplex with NDI carrying thiol units (molecular stapler).

Figure 6. (a) Image of G-quartet. (b) Various DNA quadruplex structures. (c) DNA quadruplex cluster. (d) Stacking model of NDI with DNA tetraplex from X-ray crystal

structure reported by Neidle's group [42].

Figure 7. Principle of electrochemical telomerase assay (ECTA) using FND

Figure 8. Chemical structure of the tetra- or tri-substituted (a) NDI, MM41 or (b) CM03 with its DNA quadruplex model [47] (c) Typical example of cNDI with its DNA quadruplex model (d) Chemical structure of cNDI dimer, expected the recognition of G-quadruplex cluster.

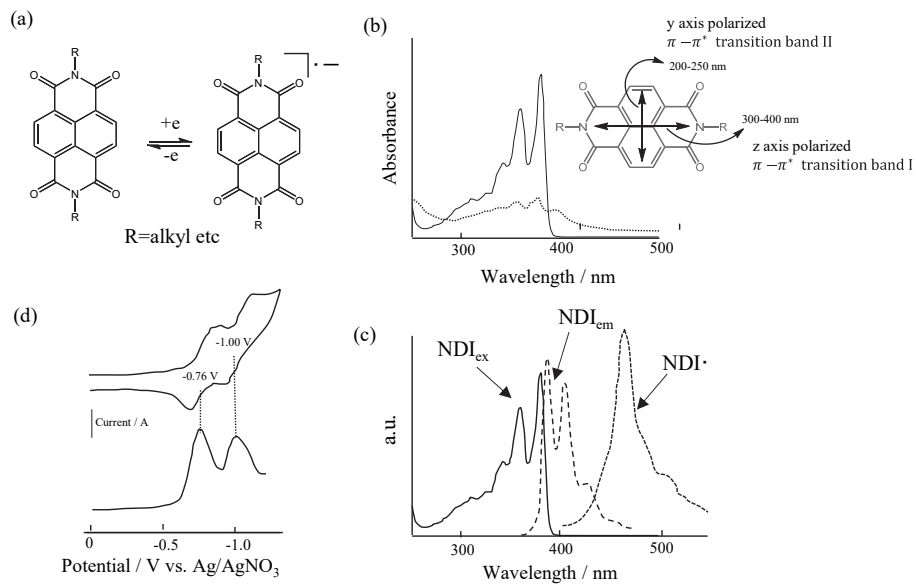


Figure 1.

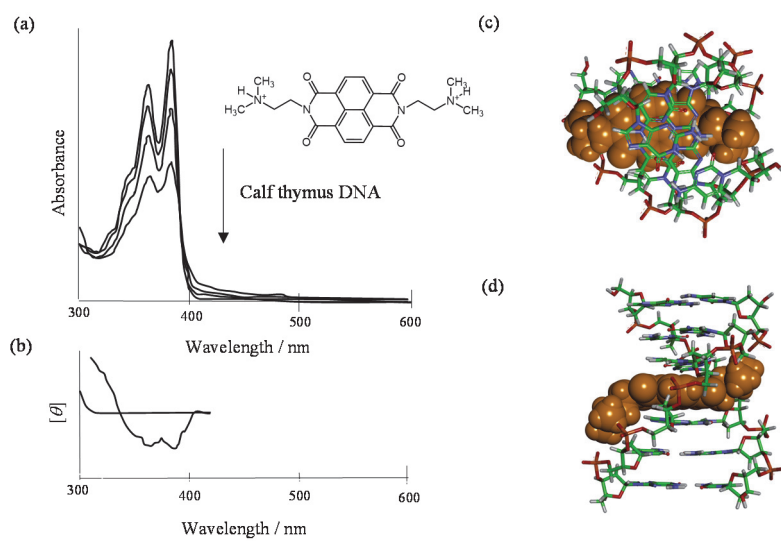
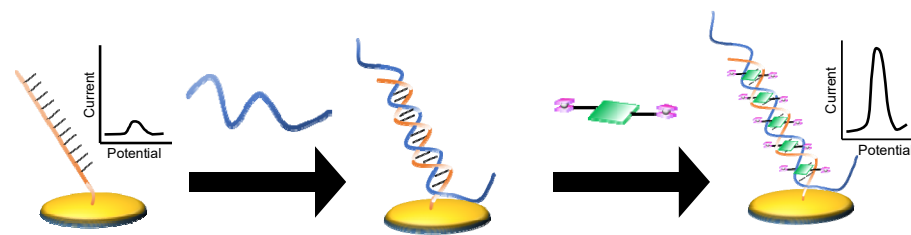


Figure 2.

Fig.3



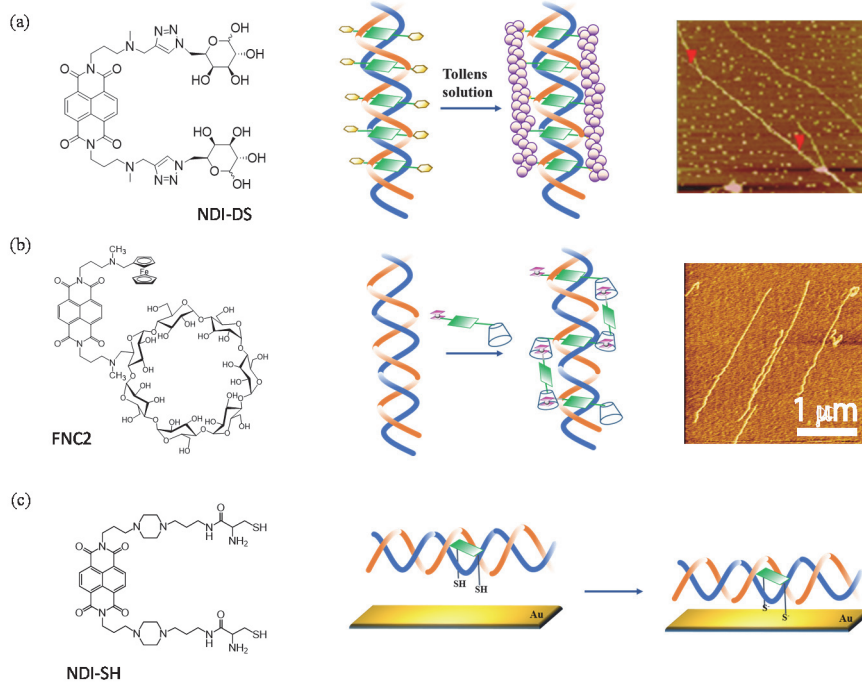


Figure 5.

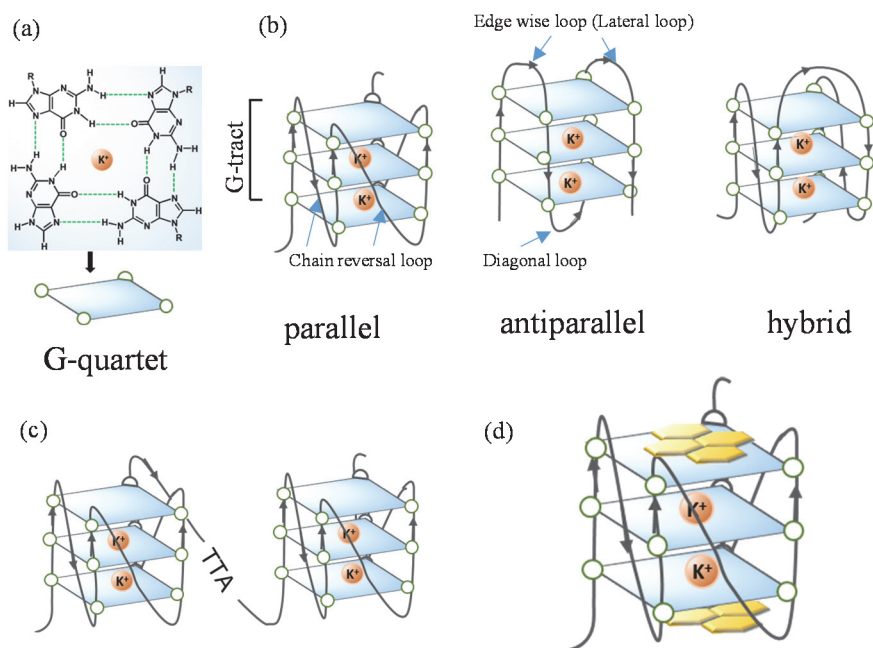


Figure 6.

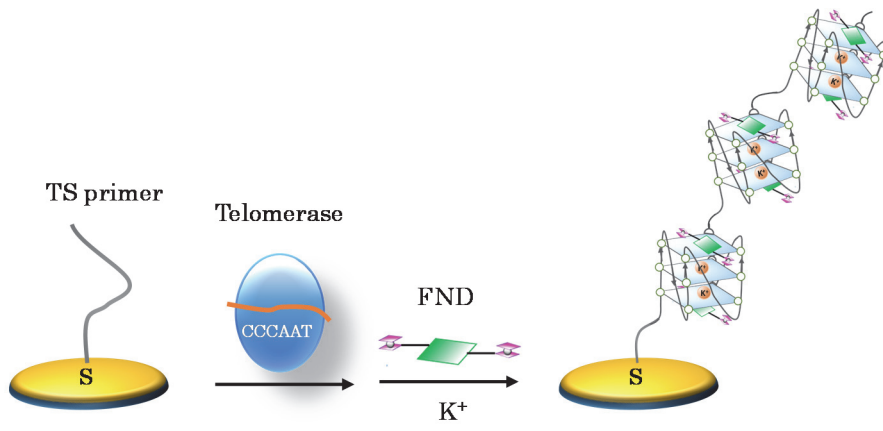


Figure 7.

Fig.8

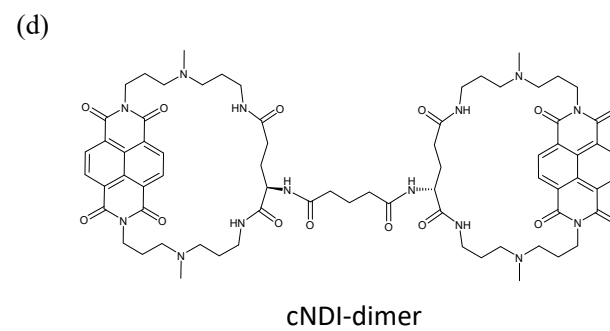
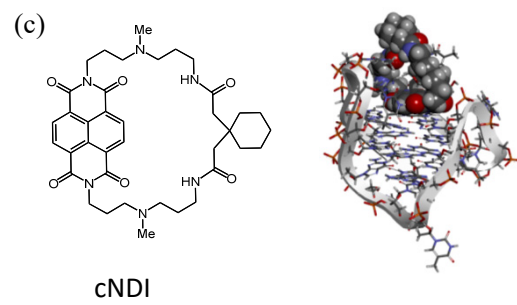
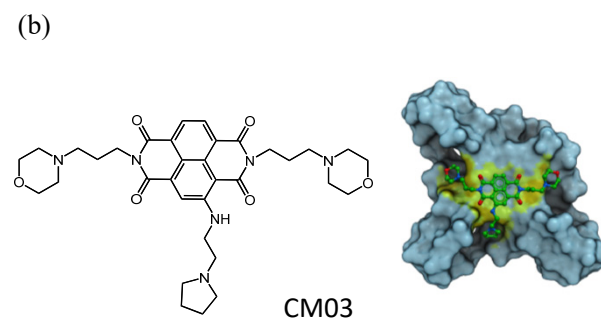
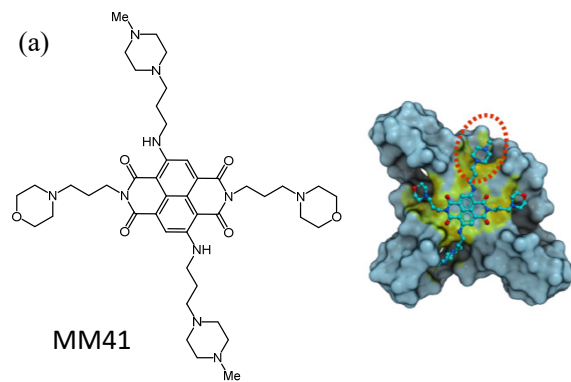
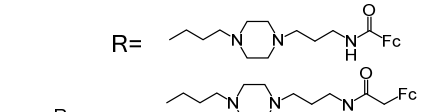
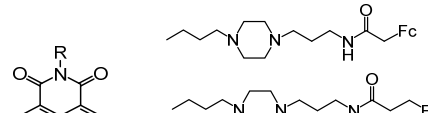
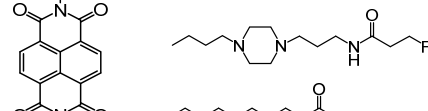
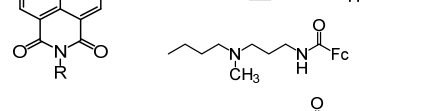
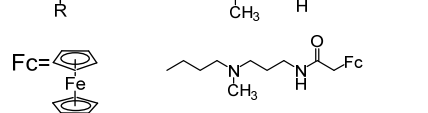
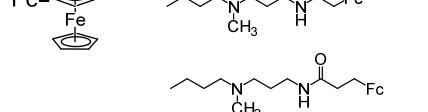
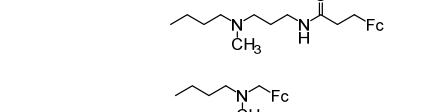
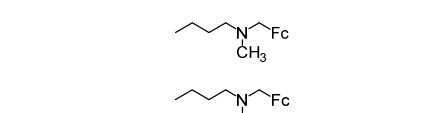
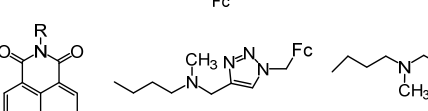
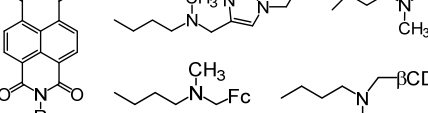
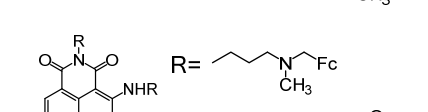
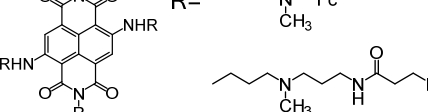
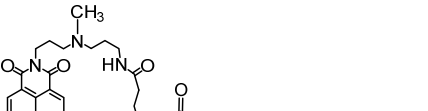
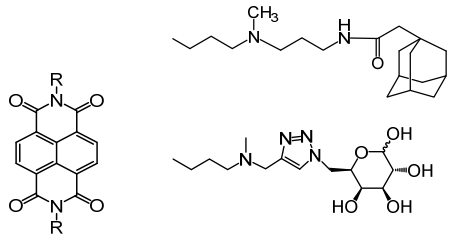
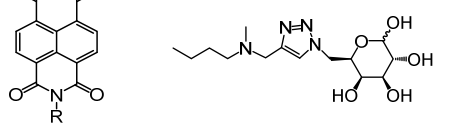
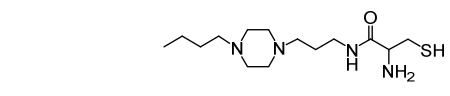
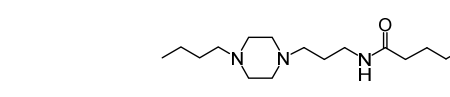
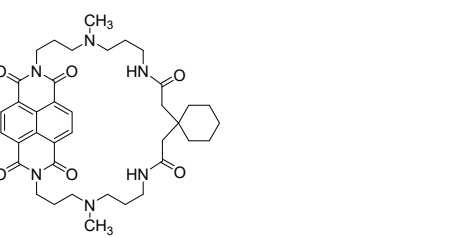
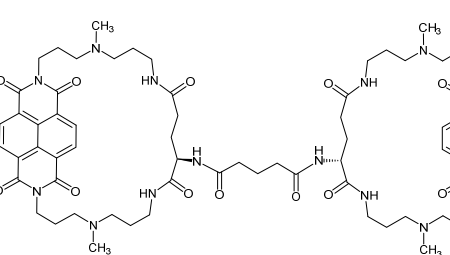


Table 1. Electroactive naphthalene diimide synthesized by Takenaka's group

Chemical Structure	Target	Affinity ($10^{-5}K/M^{-1}$)	$E_{1/2}/V$ vs. Ag/AgCl	Other
	1 ^{27,45)}	dsDNA G4	1.8 ^{a,e} 4.8 (TA-core) ^{b,e}	0.45 Electroactive hybrid indicator
	2 ^{27,45)}	dsDNA G4	1.3 ^{a,e} 2.5 (TA-core) ^{b,e}	0.25
	3 ^{27,45)}	dsDNA G4	^{a,e} 87 (TA-core) ^{b,e}	0.21
	4 ^{27,45)}	dsDNA G4	0.4 ^{a,e} 7.6 (TA-core) ^{b,e}	0.47
	5 ^{27,45)}	dsDNA G4	0.3 ^{a,e} 7.6 (TA-core) ^{b,e}	0.26 11.0 ^a
	6 ^{27,45)}	dsDNA G4	8.7 ^{a,e} 4.8 (TA-core) ^{b,e}	0.22
	7 ^{27,45)}	dsDNA G4	1.1 ^a 4.8 (TA-core) ^{b,e}	0.41
	8 ²⁸⁾	dsDNA	11.0 ^{c,e}	0.42
	FNC1 ³²⁾	dsDNA	0.9 ^{c,e}	0.4 (+dsDNA) 0.34 Electroactive hybrid indicator & Supramolecular complex
	FNC2 ³⁶⁾	dsDNA	0.7 (n=4, ω=14) ^{c,e} Electrochemical preference ^a	0.4 (+dsDNA) 0.45
	tFND1 ⁴⁹⁾	G4	G4/ssDNA=2	0.23
	tFND2 ⁴⁹⁾	G4	G4/ssDNA=14	0.26 Electroactive G4 indicator
	cFND ⁵²⁾	G4	1.5 (TA-core) ^{d,f} 8.7 (c-myc) ^{d,f}	0.22 Electroactive G4 indicator

^a0.1 M AcOH-AcOK buffer (pH5.5), 0.10 M KCl, 25°C; ^b0.1 M AcOH-AcOK buffer (pH5.5), 0.10 M KCl, 30°C; ^c10 mM MES buffer, 1.0 mM EDTA (pH6.2) 0.1 M NaCl, 25°C; ^d50 mM Tris-HCl (pH7.4), 0.1 M KCl, 25°C; ^e50 mM KH₂PO₄-K₂HPO₄ (pH7.0), 25°C. Affinity was obtained from absorption^e or ITC^f change.

Table 2. Functionalized naphthalene diimide synthesized by Takenaka's group

Chemical Structure	Target	Affinity ($10^{-5}K/M^{-1}$)	Other	
	NDI-Ad ³⁰	dsDNA	1.0 ^{a,c}	Supramolecular complex
	NDI-DS ³⁴	dsDNA	0.5 ^{a,c}	Nano-wire
	NDI-SH ³⁵	dsDNA	5.1 ^{a,c}	Molecular stapler
	NDI-Co ³³	dsDNA	0.5 ^{a,c}	IR active
	cNDI ⁵⁰	G4	15 (a-core) ^{a,f} no binding (dsOligo) ^{a,f}	G4 selective ligand
	cNDI-dimer ⁵³	G4 cluster	10 ^{b,f}	G4 cluster ligand

^a10 mM MES buffer, 1.0 mM EDTA (pH6.2) 0.1 M NaCl, 25°C; ^b50 mM Tris-HCl (pH7.4), 0.1 M KCl, 25°C. Affinity was obtained from absorption^c or ITC^f change.